Published in final edited form as:

Skeletal Radiol. 2021 May ; 50(5): 903–913. doi:10.1007/s00256-020-03625-3.

Radiographic imaging, densitometry and disease severity in Autosomal dominant osteopetrosis type 2.

Lauren M. Ladd[1,2], **Erik A. Imel**[2,3,4], **Paul J. Niziolek**[1,2], **Ziyue Liu**[2,5], **Stuart J. Warden**[2,6,7], **Yun Liang**[1], **Michael J. Econs**[2,3,8]

[1]Indiana University School of Medicine, Department of Radiology & Imaging Sciences

[2]Indiana University, Indiana Center for Musculoskeletal Health

[3]Indiana University School of Medicine, Department of Medicine

[4]Indiana University School of Medicine, Department of Pediatrics

[5]Indiana University, School of Public Health, Department of Biostatistics

[6]Indiana University, School of Health and Human Sciences, Department of Physical Therapy

[7]La Trobe University, La Trobe Sport and Exercise Medicine Centre

[8]Indiana University School of Medicine, Department of Medical and Molecular Genetics.

Abstract

OBJECTIVE: To characterize relationships between quantitative computed tomography bone mineral density measurements and other qualitative and quantitative imaging measures, as well as clinical metrics, in patients with autosomal dominant osteopetrosis type 2 (ADO2).

MATERIALS & METHODS: Clinical and radiologic parameters of 9 adults and 3 children with autosomal dominant osteopetrosis type 2 were assessed including lumbar spine quantitative computed tomography (QCT), radiographic skeletal survey [skull base thickening; Erlenmeyer flask deformity; endobone pattern; and spine density pattern (endplate sclerosis, “anvil” appearance, or diffuse sclerosis)], dual energy x-ray absorptiometry (DXA), tibial peripheral quantitative computed tomography (pQCT) volumetric bone mineral density (vBMD), bone turnover markers, and bone marrow failure or visual impairment.

RESULTS: The skeletal parameter most divergent from normal was lumbar spine QCT Z-score (+3.6 to +38.7). Lumbar QCT Z-score correlated positively with pQCT tibial diaphysis vBMD (Pearson correlation r=0.73, p=0.02) and pQCT tibial metaphysis vBMD (r=0.87, p<0.01). A trend towards positive lumbar QCT Z-score correlation with serum P1NP/CTX ratio (r=0.54, p=0.10)

Corresponding Author: Lauren M. Ladd, LMLadd@iupui.edu, 1701 N. Senate Blvd, Radiology Dept, MH1238A, Indianapolis, IN 46202.

Conflicts of Interest: The authors report no other conflicts of interest. The sponsor had no role in the study design or analysis.

COMPLIANCE WITH ETHICAL STANDARDS

Ethical approval: All procedures performed in studies involving human participants were in accordance with the ethical standards of the institutional and/or national research committee and with the 1964 Helsinki declaration and its later amendments or comparable ethical standards.

Informed consent: Informed consent was obtained from all individual participants included in the study.

and lumbar DXA Z-score (r=0.55, p=0.10) were observed. Bone marrow failure and vision impairment occurred in those with most severe quantitative and qualitative measures, while those with less severe radiographic features had the lowest QCT Z-scores.

CONCLUSION: Lumbar spine QCT provided the most extreme skeletal assessment in ADO2, which correlated positively with other radiologic and clinical markers of disease severity. Given the quantification of trabecular bone and greater variation from normal with wider range of values, lumbar QCT Z-scores may be useful to determine or detect impact of future treatments.

Keywords

osteopetrosis; ADO2; osteoclast; quantitative computed tomography

INTRODUCTION

The osteopetroses are rare genetic bone disorders resulting in osteosclerosis. Mutations in ten different genes have been reported to cause various forms of osteopetrosis, all of which impair osteoclast generation or function [1]. The most severe forms present in infancy and are autosomal recessive, while the autosomal dominant osteopetroses are less severe but still result in clinically important complications [2–4]. The most common form of osteopetrosis, autosomal dominant osteopetrosis type 2 (ADO2), was first described by radiologist Heinrich Albers-Schonberg as “marble bone disease” in the early 20th century due to diffusely increased bone density.

ADO2 is caused by mutations in the chloride channel 7 (*CLCN7*) gene [5]. Osteoclasts grown from patients with CLCN7 gene mutations demonstrate clearly impaired resorptive ability when grown on dentin matrix cultures [6–8]. ADO2 disease severity is highly variable with one third of individuals harboring CLCN7 mutations being asymptomatic carriers, and the other two thirds having mild, moderate or severe disease [4,9]. Clinical manifestations may present in childhood or not be detected until adulthood [3,10]. The majority of affected patients, 92%, experience morbidity from several complications, which may include primary complications (fracture with minor trauma, mandibular or maxillary osteonecrosis and/or osteomyelitis, and cranial nerve palsies resulting from cranial hyperostosis) and secondary complications (bone marrow failure with anemia, hepatosplenomegaly, extramedullary hematopoiesis, and risk of infection), often causing poor quality of life [4,5,11,12]. Further, the clinical phenotype does appear to worsen over time [4,13].

The resulting osteosclerotic bones are dense but brittle with classic radiographic patterns, particularly in the spine having the appearance of thickened densities involving the endplates and adjacent subcortical portions of the vertebral body alternating with comparatively less dense portions of the vertebral body centrally (rugger-jersey spine), in the pelvis and other bones having a bone-within-a-bone (“endobone”) appearance of alternating high density and comparatively less dense areas within the medullary space paralleling the cortex, and in the long bones demonstrating cortical thickening, Erlenmeyer flask deformity and/or dense metaphyseal transverse bands [11,12,14,15]. Although several investigators have described the radiographic imaging findings [11,12,14,16], dual-energy x-ray absorptiometry (DXA)

[13,17], and peripheral quantitative computed tomography (pQCT) [17] of ADO2, the optimal modality for assessing disease severity and changes over time is not known.

The aim of the current study is to document clinical, biochemical, and imaging markers in a cohort of subjects with ADO2 to characterize disease severity, explore correlations between measures of severity, and identify potential quantifiable endpoints for future clinical trials. .

MATERIALS AND METHODS

Participants

Adults and children with clinical features of ADO2, including increased bone mass and classic radiographic features, were enrolled in a pilot clinical trial [18] between July 2016 and November 2017. The current imaging data were assessed at the commencement of the parent trial. Exclusion criteria included: serum calcium >10.6 mg/dL; estimated glomerular filtration rate (eGFR) <35 mL/min/1.73m^2; nephrocalcinosis of Grade 3 or higher on screening ultrasound; use of any investigational treatment or product within 30 days prior to the study; history of hepatitis C, alcoholism, or intravenous drug abuse; presence of moderate or severe renal disease or liver disease at screening; or current pregnancy or lactation. The study was conducted in accordance with the Declaration of Helsinki and approved by the Indiana University Institutional Review Board, and monitored by an independent data safety and monitoring board (ClinicalTrials.gov # NCT02584608). Written informed assent was obtained from participants <18 years of age and written informed consent obtained from participants ≥18 years and parents/guardians of participants <18 years of age.

Imaging studies

Four imaging examinations were performed—1) skeletal survey radiographs, 2) dual-energy x-ray absorptiometry (DXA), 3) peripheral quantitative computed tomography (pQCT), and 4) axial (spine) QCT. Participants ≥15 years of age had each imaging study performed, whereas spine QCT was excluded for subjects <15 years (a total of 2 participants) to limit radiation dose.

Skeletal survey—Skeletal survey radiographs included the following radiographic views: lateral skull, AP and lateral cervical spine, AP and lateral thoracic spine, AP and lateral lumbar spine, AP pelvis, AP right and left femora, AP chest, and AP right and left humeri. Image interpretation was performed by one fellowship-trained musculoskeletal radiologist (L.M.L.). Analysis of radiographic appearance included assessment of bone involvement (skull base, spine, pelvis, long bones, ribs), skull base thickening, Erlenmeyer flask deformity, endobone pattern of sclerosis, and spine density pattern (endplate sclerosis, “anvil” appearance, or diffuse sclerosis).

DXA—Areal bone mineral density was measured for the lumbar spine (L1-L4), total hip, femur neck, and whole-body using a GE Lunar Prodigy Advance DXA scanner (Madison, WI, USA). DXA assessment of energy absorption within the projected bone area included tissue of both higher and lower densities, as is standard technique. ADO2 patients have areas

of lower density bone within the projected image, but absorption (reflecting bone density) is measured across the total area (i.e. low and high density) and compared to the same composite in 'normal' individuals. As per standard technique, visual assessment of the vertebral bodies and hip confirmed appropriate area of interest demarcation, including both dense endplates and relatively decreased mineralization centrally in vertebral bodies, as well as excluding analysis of hips with prior fractures or hardware. The underlying anatomy, as evidenced by the skeletal survey, revealed no confounding factors, such as osteophytosis, that may result in falsely elevated bone mineral density [19]. Z-scores were calculated from age, sex and race normative data using the manufacturer's software Version 13.6.

Tibial pQCT—pQCT was performed using a Stratec XCT 3000 machine (Stratec Medizintechnik GmbH, Germany), as previously described [20]. Slices (thickness = 2.3mm; voxel size = 400μm; scan speed = 20mm/s) were taken at 66% (tibial diaphysis) and 4% (distal tibia) of tibial length proximal from its distal end. Cortical mode 1 (threshold, 710 mg/cm^3) was used to obtain total and cortical volumetric bone mineral density (vBMD), bone mineral content (BMC), and area at the tibial diaphysis. Medullary area was derived as total minus cortical area. Average cortical thickness was obtained using a circular ring model with peel mode 2 (threshold, 400 mg/cm^3) to separate the cortical and subcortical/medullary compartments.

At the distal tibia, contour mode 1 (threshold, 300 mg/cm^3) was used to define the outer bone edge and peel mode 2 (threshold, 600 mg/cm^3) to separate the cortical/subcortical and trabecular compartments. Properties recorded included total vBMD, BMC and area. Short-term precision for the pQCT procedure showed root mean square coefficients of variation of <1% for density, mass, and structure measures [21]. As there is no established normative reference database for pQCT outcomes and to illustrate the extreme bone properties in individuals with ADO2, data obtained were compared to those in a cohort of athletic, healthy male controls obtained using the same scanner and protocol [20].

Lumbar QCT—The trabecular BMD was measured in the lumbar spine by QCT at L1, L2, and L3, using a 64-slice helical CT scanner (Brilliance CT 64 Channel; Philips Medical Systems, Best, the Netherlands) and QCT phantom (Image Analysis QCT-Bone Mineral™ Phantom; Image Analysis Inc, Columbia, KY). The patient was supine with the phantom beneath the patient, and CT imaging was performed with contiguous axial slices from L1 through L3 based on scout images. The following CT imaging parameters were utilized: 120 kV, 300 mAs, 2 mm slice thickness, and no dose modulation. At the center axial slice of each vertebral body, a region of interest (ROI) density measurement of each of the three components of the phantom was obtained. An elliptical ROI was also manually drawn within the vertebral body at the center axial slice of each included vertebral body (Figure 1). BMD for each vertebral body was subsequently derived from the calibration measurements. Data extracted from sex-specific healthy controls from Cann and colleagues [22] was then used to calculate the Z-score for each vertebral body.

Biochemical studies

Fasting blood and urine samples were collected for laboratory assessments and measured at Covance Inc., Analytical Services Central Laboratory (Indianapolis, Indiana) [18]. Only values from the baseline study visit are presented here. Assays included serum C-telopeptide (CTX) measured using the Beta-Cross-Laps assay (Elecsys electrochemiluminescence immunoassay, Roche Diagnostic), urine N-telopeptide (NTX) ELISA (Osteomark, Ostex International Inc., Seattle, Wa), and serum procollagen type I N-terminal propeptide (P1NP; Electrochemiluminescent immunoassay, Roche Diagnostic). Biochemistries, including urine creatinine, were measured using Roche Cobas 8000 (Indianapolis, IN) clinical analyzers. The simple ratio of NTX to creatinine was calculated to adjust for urine concentration. The simple ratio of P1NP to CTX was calculated to assess the relative contribution of bone formation to bone resorption markers.

Clinical assessment

Clinical parameters indicating disease severity were recorded from the patient's medical record and evaluation by two endocrinologists (M.J.E. and E.A.I.) with subspecialty expertise in osteopetrosis evaluation and management. Clinical markers of disease severity included visual impairment (blindness or prior operative management of skull base involvement to preserve vision) and evidence of bone marrow failure (ranging from mild anemia to severe anemia with transfusion-dependence or pancytopenia).

Statistical analysis

Categorical variables were summarized by counts and percentages. Continuous variables were summarized by mean, standard deviation, and range when appropriate. Pearson correlation coefficients were used to quantify the associations between continuous variables in the primary analysis. Spearman's correlation coefficients were also generated as sensitivity analysis.

RESULTS

Participants and Clinical assessment

All 12 screened participants were included. Mean age was 30.7 years (range 8 to 50 years old), including 3 children (ages 8.1, 9.6 and 15.9 years). The cohort included 6 male and 6 female participants; and 11 white and 1 African American participants. Six of the 12 participants (50%) had vision impairment due to ADO2, including two children that had skull base surgery to prevent or limit optic nerve impairment, and 3 with blindness in one or both eyes. Additionally, blood cell analysis indicated varying degrees of bone marrow failure resulting in anemia in 7/12 (58%), low white blood cell counts in 4/12 (33.3%) and low platelet counts in 2/12 (16.7%). The participant with the most severe bone marrow failure in this study was transfusion-dependent. Four participants (33.3%) had both anemia and vision loss.

Imaging Studies:

Skeletal Survey—Radiographic skeletal surveys demonstrated that each participant had at least four of the five classic features of ADO2, including: osteosclerosis (including cortical thickening or diffuse increased bone density), skull base thickening and sclerosis, and Erlenmeyer flask deformity, endobone appearance, and vertebral body endplate sclerosis (Figure 2). Seven participants demonstrated all five features (Table 1). Three distinct vertebral body patterns were also noted, which in order of increasing severity were: 1) sclerotic endplates without central increased density (rugger-jersey spine), 2) endplate sclerosis with central density ("anvil" appearance), and 3) diffuse sclerosis (Figure 3). Two had the least severe pattern of only sclerotic endplates of the vertebral bodies, 7 had the "anvil" appearance (of which two were only mild), and 3 had diffuse sclerosis.

DXA—Areal BMD was highly elevated at all sites (Table 1). When compared to age-, sex-, and race-matched healthy normal individuals, the ADO2 participants had much greater energy absorption (i.e., higher composite bone density) within the projected bone area. The DXA Z-score ranges (means) were +4.7 to +15.5 (+11.8) for the lumbar spine, +2.8 to +20.2 (+12.5) for the femoral neck, +5.1 to +17.2 (+12.8) for the total hip, and +4.2 to +17.8 (+10.6) for the whole-body.

Tibial pQCT—pQCT of the tibial diaphysis and distal tibia revealed relatively solid bones with limited to no marrow cavity (Figure 4). When compared to healthy, young male athletes, all ADO2 participants had elevated total and cortical vBMD and BMC with mean Z-scores ranging from +2.5 to +6.0 (Table 2). Despite lower overall bone cross-sectional size (i.e. total area), cortical area and thickness were larger in ADO2 participants compared to healthy, young male athletes due to reduced medullary area. Calculating the ratio of cortical-to-medullary area yielded a mean Z-score of +37.7 for ADO2 participants compared to healthy, young male athletes. Similar findings were observed at the distal tibia with total vBMD and BMC being elevated in ADO2 participants relative to healthy, young male athletes, while bone cross-sectional size was smaller (i.e. total area).

Lumbar QCT—Lumbar QCT revealed elevated bone mineral density, ranging from 267.0 to 1130.0 mg/cm^3 (mean 726.6 mg/cm^3). Corresponding Z-scores ranged from +3.6 to +35.7 (mean +19.7, Table 1).

Biochemical analysis results:

The full biochemical analysis in these participants was previously published [18]. Briefly, all participants had normal age-appropriate serum calcium, phosphorus, total alkaline phosphatase and creatinine, and low fasting urine calcium/creatinine ratio. All participants also had normal serum CTX and urine NTX/creatinine ratio except for one participant having a low NTX/creatinine ratio. 7/12 participants (58.3%) had elevated P1NP, while 4/12 (33.3%) had P1NP in the upper normal range. Children had higher bone turnover marker levels than adults.

Correlation analysis

Pearson correlation coefficients are presented to demonstrate the relationship between measured parameters. Spearman correlation coefficients were similar hence not presented. Age did not correlate with any of the skeletal radiograph or BMD assessments. However, as graphically represented in Figures 5, bone marrow failure and vision impairment generally was seen in those participants with more severe radiographic, DXA, pQCT, and QCT measures.

The three participants with the least severe radiographic features on skeletal survey (all adults) also had the lowest spine QCT measurements (Z-scores of +3.6, +8.1, and +10) of the participants in this study. QCT was not able to differentiate between participants with four versus five radiographic features. However, the vertebral body pattern on radiographs corresponded well to the QCT Z-score severity ($r=0.96$, $p<0.0001$). The two participants with classic “rugger jersey” vertebral body sclerosis pattern have Z-scores <10, whereas the two most subtle “anvil” patterns correlated with Z-scores between 10–20, the remaining five more dense “anvil” patterns correlated with Z-scores between 20–30, and the two participants with diffuse sclerosis correlated with Z-scores of >30. Other radiographic findings did not correlate with higher QCT Z-scores.

Figure 5 illustrates that among ADO2 participants, there is a general positive correlation between DXA measurements and QCT in these participants. QCT spine correlated positively with spine DXA ($r=0.55$, $p=0.10$) and total body Z-scores ($r=0.81$, $p<0.01$), though only the total body Z-score reached statistical significance. Of note, lumbar QCT Z-scores exceeded DXA Z-scores for lumbar spine in 7 of 10 participants (70%) and for total body in 8 of 10 (80%). In several cases, the lumbar QCT Z-scores markedly exceeded DXA Z-scores, indicating greater separation from normal by QCT compared to DXA.

Lumbar QCT Z-scores also positively correlated with tibial diaphyseal pQCT total volumetric BMD ($r=0.73$, $p=0.02$) and distal tibial pQCT total volumetric BMD ($r=0.87$, $p=0.001$). This is graphically depicted in Figure 5 (a-c).

Finally, there is a trend towards positive correlation between bone turnover markers (P1NP/CTX ratio) and lumbar QCT as demonstrated in Figure 5d ($r=0.54$, $p=0.10$).

DISCUSSION:

This study describes and compares detailed radiographic and densitometric assessment of participants with autosomal dominant osteopetrosis type 2 and describes positive correlations among different potential clinical and radiographic markers of disease severity. Variation in severity of radiographic and densitometric features among participants were observed. Different from previous report of varying severity, broadly categorized as “carrier,” “moderate,” and “severe” based on clinical manifestations by Waguespack, et al[4], this study demonstrates detailed quantitative and qualitative differences among subjects. Notably, this study reveals Z-scores from lumbar QCT assessment were more extreme than other measures and were associated with important clinical consequences such

as anemia and vision impairment. In addition, this study provides the first description of variation in disease severity using the radiographic pattern of vertebral body sclerosis.

QCT is a useful technique to accurately assess BMD, particularly in disease processes where cortical bone mineralization or artifacts, such as osteophytes or fractures, may affect DXA BMD measurements. In a prior study using DXA as gold standard of BMD, QCT measurements in healthy adults yielded slightly lower BMD than DXA, though by a small and relatively consistent margin that could be adjusted for to use DXA reference data for clinical decision making with QCT results [23]. Another study comparing QCT and DXA measurements in postmenopausal women with osteoporosis by DXA demonstrated greater accuracy and lower overall BMD by QCT because it avoids measurement overestimation from confounding factors, such as degenerative disease, abdominal aortic atherosclerotic calcifications, or other sclerotic lesions [24]. There are no prior studies comparing QCT and DXA in osteosclerotic bone disease; however, from the aforementioned studies and with an understanding of QCT technique [25], it may be most useful for accurate assessment of disease severity in sclerotic bones because it measures the trabecular bone (unobstructed by cortical density or artifacts) [25,26] and yields measurements furthest from normal ranges. As trabecular bone has higher metabolic activity and the wider range of measurements produced, this technique may be most sensitive for detecting changes in density [25,27]. For this reason, we assessed the correlation of QCT bone mineral density measurements with multiple radiographic and other imaging study results, as well as with biochemical and clinical markers of disease severity.

On radiographs, as seen in Figure 2, osteopetrosis is characterized by osteosclerosis or dense bones with classic features including the following: (1) diffuse sclerosis affecting the skull, spine, pelvis, and appendicular bones; (2) abnormally widened long bone metaphyses, called “Erlenmeyer flask deformity”; (3) endobone, or “bone-in-bone,” appearance of the axial and appendicular skeleton, including phalanges; (4) skull base thickening and sclerosis; and (5) vertebral end plate sclerosis, resulting in a pattern similar to that of a rugby jersey and consequently referred to as “rugger-jersey” spine [3,9,28].

Three distinct variations of the vertebral body sclerosis pattern were evident, all of which demonstrate some degree of the “rugger jersey” spine. The first and seemingly least severe pattern is the classic dense sclerotic bands at the vertebral body endplates (ie, the classic “rugger jersey” spine) (Figure 3a). The second pattern demonstrates greater severity with an additional central vertebral body sclerotic region connecting the superior and inferior endplate sclerotic bands, described here as the “anvil” appearance (Figure 3b). Finally, the most severe pattern of sclerosis is the diffusely sclerotic vertebral body (Figure 3c), which corresponded with the greatest QCT Z-scores. Given the strong correlation with QCT Z-scores, it is apparent that the vertebral body sclerosis pattern may help predict severity of disease radiographically.

Lumbar QCT Z-scores were also noted to exceed DXA Z-scores in 8 of 10 participants for whole body DXA measurements and 7 of 10 participants for lumbar spine DXA measurements with QCT Z-scores equal to or less than DXA Z-scores in only the least severely affected participants. In some cases, QCT markedly exceeded DXA Z-scores (Table

1 and Figure 2), indicating greater separation from normal by QCT compared to DXA. The larger deviation from normal combined with the wider range of values seen by lumbar QCT may make this a better quantitative metric to follow in a study designed to look at change in density over time, either to further determine worsening of ADO2 over time or to assess the effect of a potential therapy.

Osteoclast dysfunction is key to the pathophysiology of ADO2, but other bone cell types may be involved in the skeletal phenotype. Frequently in conditions suppressing bone resorption (such as bisphosphonate administration), the bone formation is also suppressed [29]. However, in the prior publication from this ADO2 study population, CTX and NTX/Cr (measures of bone resorption) were in the low normal range for most subjects, while Procollagen type I N-terminal propeptide (P1NP) (measure of bone formation) was elevated or in the upper normal range in 11/12 (91.6%) subjects [18]. The ratio of bone formation over resorption markers (P1NP/CTX) is now also shown to be positively related to lumbar QCT Z-score, as well as DXA and tibial pQCT in ADO2. This relationship of high bone formation markers to density in ADO2 suggests that the osteosclerosis is not merely due to impaired resorption, but is also accompanied by increased (or at least preserved) bone formation [18]. While increased bone formation markers were not seen in the ADO2 mouse model [30], preserved bone formation would potentially support the generally normal growth and skeletal size among patients with ADO2, as well as the development of the classic metaphyseal shape abnormalities during growth [18]. Thus, osteocytic or osteoblastic functions may contribute to the sclerosis through effects on bone formation. A bone biopsy case series suggested osteocytic osteolysis may also contribute to the osteosclerotic features of osteopetrosis, though the genotype in in that study is not known [31]. A limitation of our study is a lack of bone biopsy analysis to more fully evaluate the contribution of bone formation to the radiographic phenotype.

Lastly, several clinical markers of severity also corresponded to bone mineral density markers as noted in Figure 5. Two clinical findings that cause significant morbidity in patients with ADO2 are vision impairment due to skull base thickening and nerve impingement and bone marrow failure, resulting in a spectrum of anemia to fulminant bone marrow failure. The latter is a cause of premature death in patients with ADO2. These clinical markers of severity were not always simultaneously present but did demonstrate a tendency to occur in those who had highest lumbar QCT Z-scores, as well as greater tibial pQCT and DXA Z-scores, indicating either complication is a significant indicator of disease severity and should be closely monitored.

Strengths of this study include a detailed multimodal assessment of patients with severe features of ADO2 and inclusion of both adults and children. Limitations include that the study sample was small, which limits statistical power. Although other imaging and clinical data were not known at the time of interpretation, skeletal radiographs were assessed by only one radiologist, potentially contributing to error based on subjectivity. This study also lacks longitudinal assessments. The subjects were recruited as part of a 14-week pilot clinical trial for interferon gamma-1b treatment. However, 14 weeks was deemed too short to expect to see changes in BMD, and since that trial did not demonstrate effects on bone resorption markers and had significant side effects, the treatment period was not extended [18]. Finally,

additional quantitative imaging, such as high resolution peripheral QCT (HRpQCT) were not employed, which may also be promising in determining treatment response with lower radiation dose in future studies and practice.

In summary, this study demonstrates varying radiographic features as well as lumbar QCT values in patients with severe manifestations of ADO2. These results suggest that lumbar QCT, DXA, and tibial pQCT all demonstrate abnormal bone mineral density measures to indicate severity of disease, though the lumbar QCT may be the best tool for assessing severity and potentially change over time. Ultimately, these measurements may be useful in characterizing disease severity and evaluating effects of novel therapies in future clinical trials to assess medical therapies for autosomal dominant osteopetrosis type 2.

Acknowledgments

Funding Sources: This study was funded in part by a grant from Horizon Pharmaceuticals, and was also supported by the National Institutes of Health through NIAMS grant P30AR072581 (The Indiana Center for Musculoskeletal Health Clinical Research Cores), NIAMS grant R01AR077869, and by the NCATS award UL1TR002529 (The Indiana Clinical and Translational Sciences Institute). The content is solely the responsibility of the authors and does not necessarily represent the official views of the National Institutes of Health or Horizon Pharmaceuticals.

REFERENCES

1. Teti A, Econs MJ. Osteopetroses, emphasizing potential approaches to treatment. Bone. 2017;102:50–9. [PubMed: 28167345]
2. Sobacchi C, Schulz A, Coxon F, Villa A, Helfrich M. Osteopetrosis: genetics, treatment, and new insights into osteoclast function. Nat Rev Endocrinol. 2013;9:522–36. [PubMed: 23877423]
3. Bollerslev J, Henriksen K, Nielsen MF, Brixen K, Hul WV. Autosomal dominant osteopetrosis revisited: lessons from recent studies. Eur J Endocrinol. 2013;169:R39–57. [PubMed: 23744590]
4. Waguespack SG, Hui SL, DiMeglio LA, Econs MJ. Autosomal Dominant Osteopetrosis: Clinical Severity and Natural History of 94 Subjects with a Chloride Channel 7 Gene Mutation. J Clin Endocrinol Metab. 2007;92:771–8. [PubMed: 17164308]
5. Cleiren E, Bénichou O, Van Hul E, Gram J, Bollerslev J, Singer FR, et al. Albers-Schönberg disease (autosomal dominant osteopetrosis, type II) results from mutations in the ClCN7 chloride channel gene. Hum Mol Genet. 2001;10:2861–7. [PubMed: 11741829]
6. Chu K, Snyder R, Econs MJ. Disease Status in Autosomal Dominant Osteopetrosis Type 2 Is Determined by Osteoclastic Properties. J Bone Miner Res. 2006;21:1089–97. [PubMed: 16813529]
7. Henriksen K, Gram J, Schaller S, Dahl BH, Dziegiel MH, Bollerslev J, et al. Characterization of Osteoclasts from Patients Harboring a G215R Mutation in ClC-7 Causing Autosomal Dominant Osteopetrosis Type II. Am J Pathol. 2004;164:1537–45. [PubMed: 15111300]
8. Del Fattore A. Clinical, genetic, and cellular analysis of 49 osteopetrotic patients: implications for diagnosis and treatment. J Med Genet. 2005;43:315–25. [PubMed: 16118345]
9. Stark Z, Savarirayan R. Osteopetrosis. Orphanet J Rare Dis. 2009;4:5. [PubMed: 19232111]
10. Johnston CC, Lavy N, Lord T, Vellios F, Merritt AD, Deiss WP. Osteopetrosis. A Clinical, Genetic, Metabolic, and Morphologic Study of the Dominantly Inherited, Benign Form. Medicine (Baltimore). 1968;47:149–67. [PubMed: 4871758]
11. Benichou OD, Laredo JD, De Vernejoul MC. Type II autosomal dominant osteopetrosis (Albers-Schönberg disease): clinical and radiological manifestations in 42 patients. Bone. 2000;26:87–93. [PubMed: 10617161]
12. Kant P, Sharda N, Bhowate RR. Clinical and Radiological Findings of Autosomal Dominant Osteopetrosis Type II: A Case Report. Case Rep Dent. 2013;2013:1–8.

13. Grodum E, Gram J, Brixen K, Bollerslev J. Autosomal dominant osteopetrosis: Bone mineral measurements of the entire skeleton of adults in two different subtypes. Bone. 1995;16:431–4. [PubMed: 7605703]
14. Williams HJ, Davies AM, Chapman S. Bone within a bone. Clin Radiol. 2004;59:132–44. [PubMed: 14746782]
15. Gregson CL, Hardcastle SA, Cooper C, Tobias JH. Friend or foe: high bone mineral density on routine bone density scanning, a review of causes and management. Rheumatology. 2013;52:968–85. [PubMed: 23445662]
16. Hamdan A-LH, Nabulsi MM, Farhat FT, Haidar RK, Fuleihan NS. When bone becomes marble: head and neck manifestations of osteopetrosis. Paediatr Child Health. 2006;11:37–40. [PubMed: 19030245]
17. Arruda M, Coelho MCA, Moraes AB, de Paula Paranhos-Neto F, Madeira M, Farias MLF, et al. Bone Mineral Density and Microarchitecture in Patients With Autosomal Dominant Osteopetrosis: A Report of Two Cases. J Bone Miner Res. 2016;31:657–62. [PubMed: 26387875]
18. Imel EA, Liu Z, Acton D, Coffman M, Gebregziabher N, Tong Y, et al. Interferon Gamma-1b Does Not Increase Markers of Bone Resorption in Autosomal Dominant Osteopetrosis. J Bone Miner Res. 2019;34:1436–45. [PubMed: 30889272]
19. Lorente-Ramos R, Azpeitia-Armán J, Muñoz-Hernández A, García-Gómez JM, Díez-Martínez P, Grande-Bárez M. Dual-Energy X-Ray Absorptiometry in the Diagnosis of Osteoporosis: A Practical Guide. Am J Roentgenol. 2011;196:897–904. [PubMed: 21427343]
20. Weatherholt AM, Warden SJ. Tibial Bone Strength is Enhanced in the Jump Leg of Collegiate-Level Jumping Athletes: A Within-Subject Controlled Cross-Sectional Study. Calcif Tissue Int. 2016;98:129–39. [PubMed: 26543032]
21. Swinford RR, Warden SJ. Factors affecting short-term precision of musculoskeletal measures using peripheral quantitative computed tomography (pQCT). Osteoporos Int. 2010;21:1863–70. [PubMed: 20052457]
22. Cann CE, Genant HK, Kolb FO, Ettinger B. Quantitative computed tomography for prediction of vertebral fracture risk. Bone. 1985;6:1–7. [PubMed: 3994856]
23. Khoo BCC, Brown K, Cann C, Zhu K, Henzell S, Low V, et al. Comparison of QCT-derived and DXA-derived areal bone mineral density and T scores. Osteoporos Int. 2009;20:1539–45. [PubMed: 19107384]
24. Li N, Li X, Xu L, Sun W, Cheng X, Tian W. Comparison of QCT and DXA: Osteoporosis Detection Rates in Postmenopausal Women. Int J Endocrinol. 2013;2013:1–5.
25. Link TM, Lang TF. Axial QCT: clinical applications and new developments. J Clin Densitom Off J Int Soc Clin Densitom. 2014;17:438–48.
26. Block JE, Smith R, Glueer C-C, Steiger P, Ettinger B, Genant HK. Models of spinal trabecular bone loss as determined by quantitative computed tomography. J Bone Miner Res. 1989;4:249–257. [PubMed: 2728928]
27. Ott SM. Cortical or Trabecular Bone: What's the Difference? Am J Nephrol. 2018;47:373–5. [PubMed: 29788030]
28. Sit C, Agrawal K, Fogelman I, Gnanasegaran G. Osteopetrosis: Radiological &Radionuclide Imaging. Indian J Nucl Med. 2015;30:55. [PubMed: 25589808]
29. Iizuka T, Matsukawa M. Potential excessive suppression of bone turnover with long-term oral bisphosphonate therapy in postmenopausal osteoporotic patients. Climacteric. 2008;11:287–95. [PubMed: 18645694]
30. Alam I, McQueen AK, Acton D, Reilly AM, Gerard-O'Riley RL, Oakes DK, et al. Phenotypic severity of autosomal dominant osteopetrosis type II (ADO2) mice on different genetic backgrounds recapitulates the features of human disease. Bone. 2017;94:34–41. [PubMed: 27746321]
31. Krook L, Whalen JP, Dorfman HD, Norman A, Nunez EA. Osteopetrosis: An interpretation of its pathogenesis. Skeletal Radiol. 1981;7:185–9. [PubMed: 7330675]

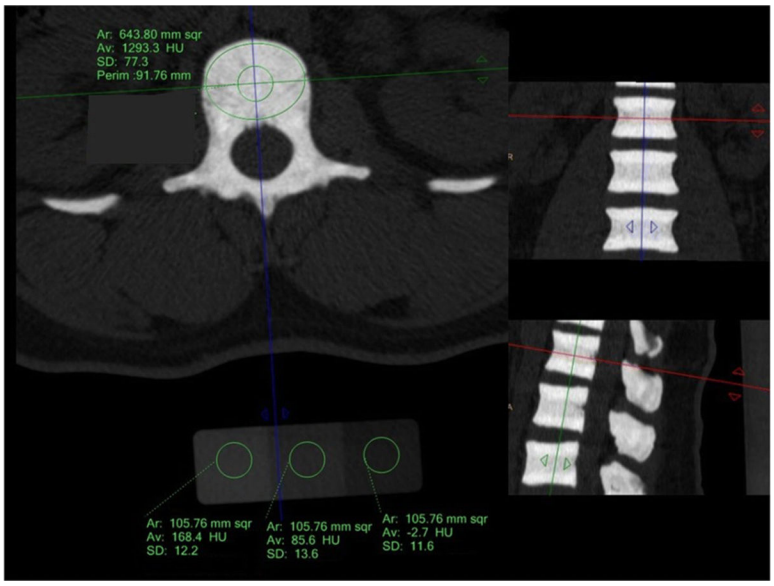

Fig. 1.

Lumbar QCT measurement technique with elliptical region of interest (ROI) manually drawn within the L1 vertebral body and circular ROIs within each of the three components of the calibration phantom.

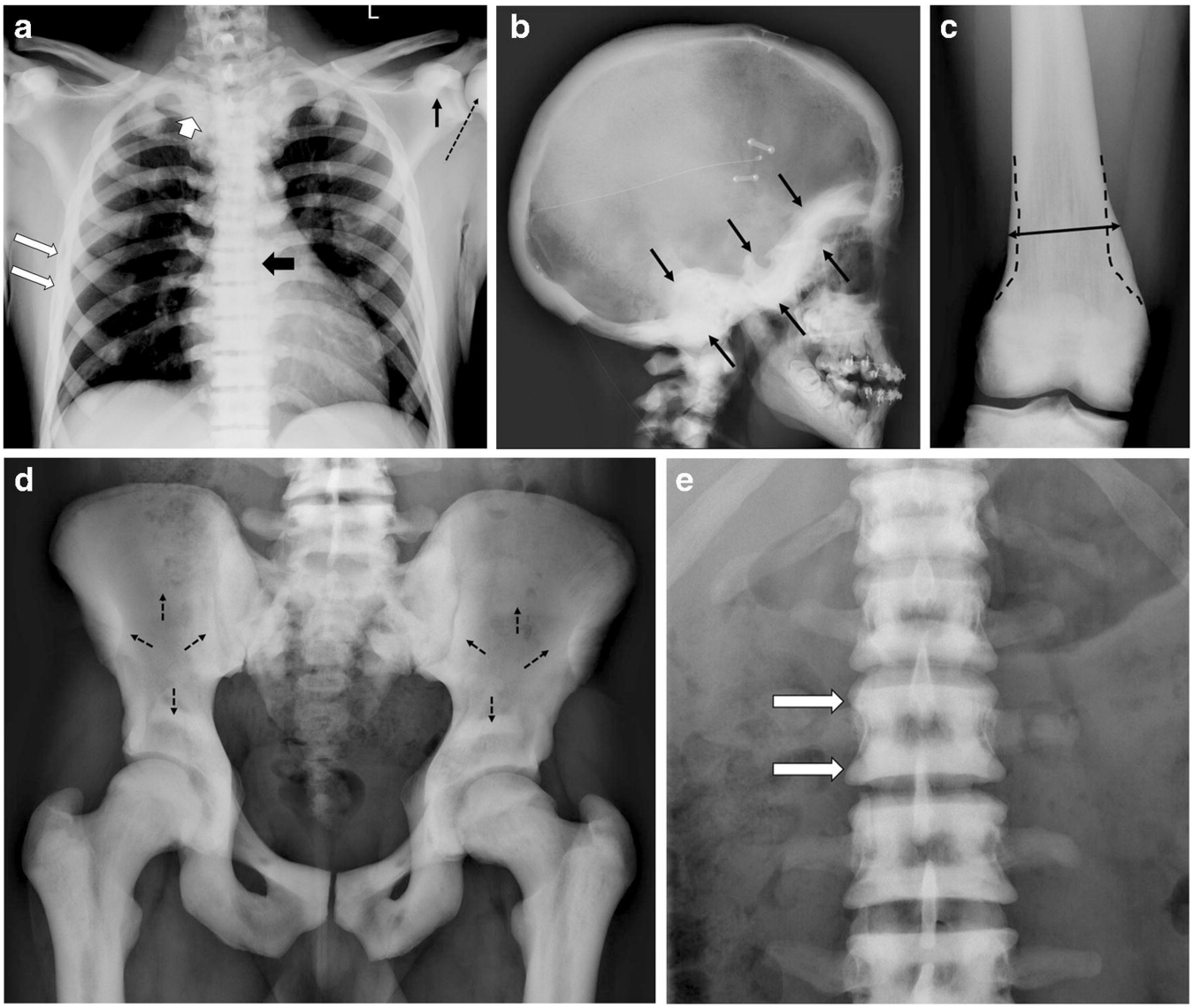

Fig. 2.

A young adult male with ADO2 demonstrates all classic radiograph features of the disease. (a) AP chest radiograph with diffuse sclerosis of the ribs (long white arrows), clavicles (short white arrow), vertebral bodies (short black arrow), coracoids (thin black arrow), and proximal humerus (dashed black arrow). (b) Lateral skull radiograph with skull base thickening (black arrows). (c) AP distal femur radiograph with Erlenmeyer flask deformity (abnormal width of distal femoral metadiaphysis, double headed arrow; expected shape of distal femur, dashed black line). (d) AP pelvis radiograph with endobone (bone-within-bone) appearance (dashed arrows). (e) AP lumbar spine radiograph with dense sclerotic bands at the vertebral body endplates (“rugger jersey” spine, white arrows).

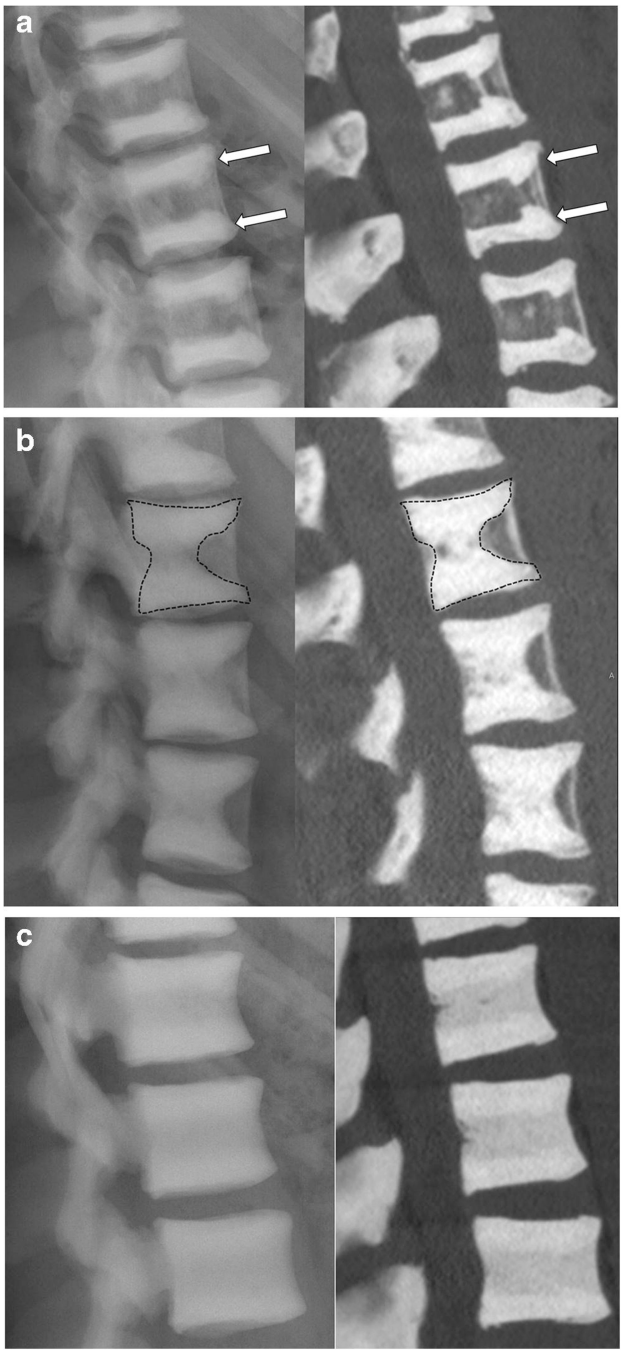

Fig. 3.

Example radiographs and CT images of each vertebral body sclerosis pattern, including (a) a middle-aged woman with the classic “rugger jersey” pattern of vertebral body sclerosis (parallel bands of increased density at the vertebral body endplates, white arrows), (b) a young adult woman with the “anvil” pattern of vertebral body sclerosis (dense sclerotic bands at the vertebral body endplates with additional central vertebral body intramedullary density, dotted outline), and (c) a middle-aged man with diffuse vertebral body sclerosis.

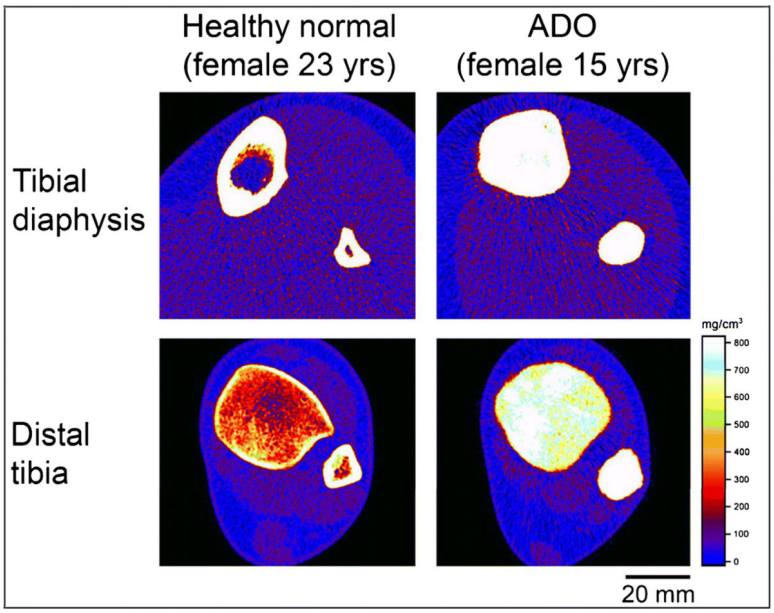

Fig. 4.

pQCT comparison of the tibial diaphysis and distal tibia in a healthy young adult control on left, and a teenage female ADO2 patient on the right, demonstrating cortical thickening and limited marrow cavity space in the osteopetrosis patient.

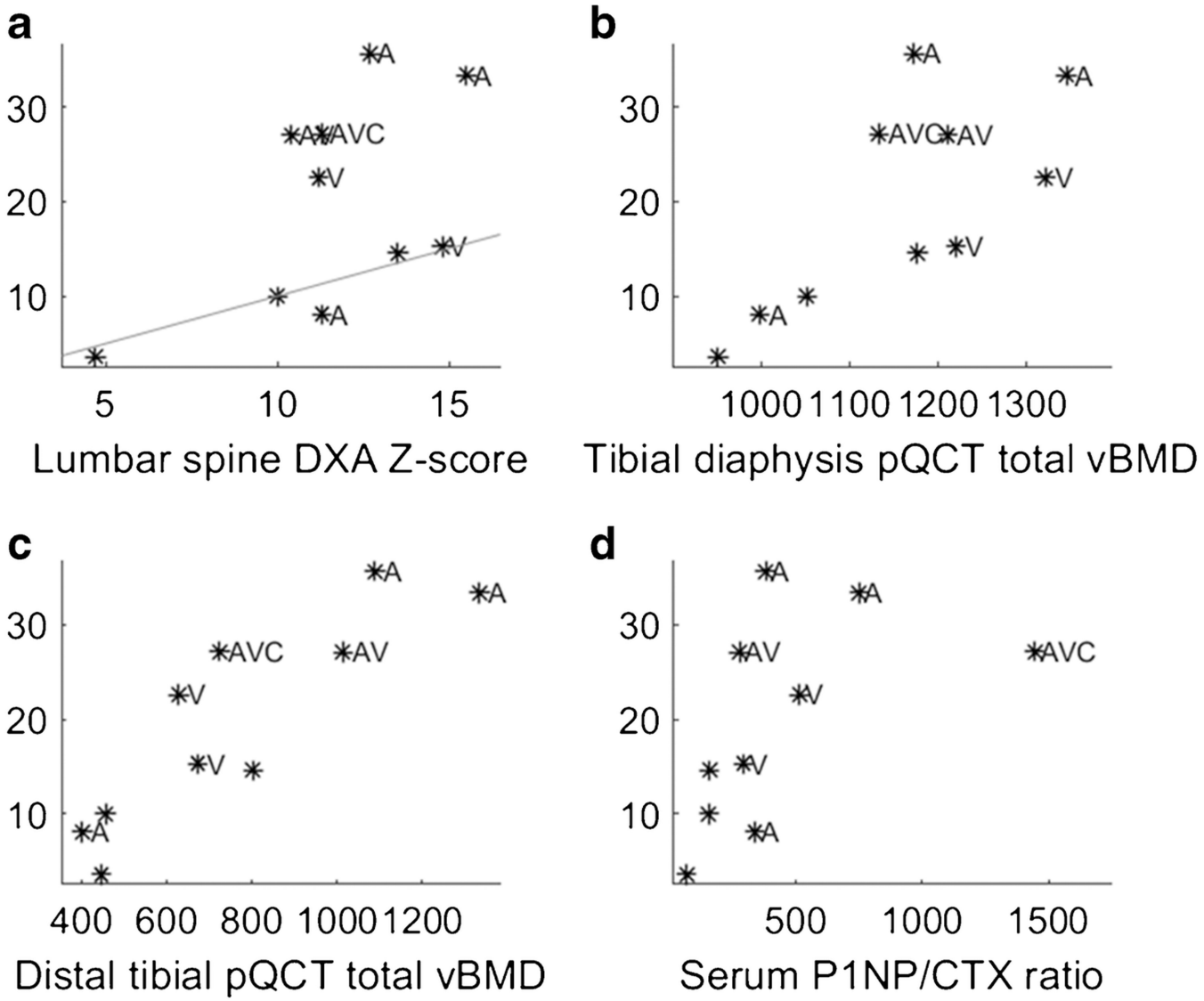

Fig. 5.

Scatter plots of lumbar spine QCT Z-score (y-axis) versus: (a) lumbar spine DXA Z-score, (b) tibial diaphysis pQCT total volumetric bone mineral density (vBMD, g/cm3), (c) distal tibial pQCT total vBMD (g/cm3), and (d) serum P1NP/CTX ratio. The data point labels of clinical metrics include anemia (A), vision impairment (V), and child (C). The solid line in (a) is the identity line that y=x, which shows that QCT Z-scores were higher than DXA Z-scores for majority of the data points.

Table 1.

Radiographic features and bone density (lumbar QCT and DXA) Z-scores of each patient

Subject	Age years	Osteosclerosis distribution	Skull base thickening	Erlenmyer flask deformity	Endobone appearance	Vertebral sclerosis pattern	QCT Lumbar Z-score	DXA Total Body Z-score	DXA Lumbar Z-score	DXA Total hip Z-score	DXA Femur neck Z-score
1	50.8	All	Yes	Yes	No	Diffuse	+35.7	+14	+12.7	+14.2	+12.9
2	42.4	All	Yes	Yes	Yes	Anvil	+27.1	+9.8	+10.4	+15.8	+14.5
3	15.9	All	Yes	Yes	Yes	Anvil	+27.2	+10.0	+11.3	N/A	N/A
4	50.3	Axial+	No	Yes	Yes	Endplates	+8.1	+8.8	+11.3	+11.6	+9.3
5	27.3	All	Yes	Yes	Yes	Anvil (mild)	+14.6	+10.8	+13.5	+13.4	+12.6
6	24.5	Axial+	Yes	Yes	Yes	Anvil (mild)	+10.0	+6.9	+10.0	+9.3	+9.4
7	9.6	All	Yes	Yes	Yes	Anvil	N/A	+11.9	+12.4	+17.0	+16.9
8	8.1	All	Yes	Yes	Yes	Anvil	N/A	+13.2	+14.1	+15.5	+16.3
9	46.4	All	Yes	Yes	No	Diffuse	+33.4	+17.8	+15.5	+17.2	+20.2
10	41.0	Axial+	Yes	No	Yes	Endplates	+3.6	+4.2	+4.7	+5.1	+2.8
11	27.5	All	Yes	Yes	Yes	Anvil	+22.6	+9.0	+11.2	+12.7	+12.7
12	21.9	All	No	Yes	Yes	Anvil	+15.3	+10.3	+14.8	+9.3	+9.4
Mean or n (%)	30.5		10 (83%)	11 (92%)	10 (83%)		+19.7	+10.6	+11.8	+12.8	+12.5

All = diffuse skeletal involvement, Axial+ = spine, pelvis, and proximal long bones; Anvil = endplate sclerotic bands with central intramedullary sclerosis, Endplates = dense sclerotic bands at the vertebral body endplate

Table 2.

Bone density, mass, structure and estimated strength at the tibial diaphysis and distal tibia in the legs of athletic, healthy male controls and participants with autosomal dominant osteopetrosis (ADO2)

	Control[ab]	ADO[a]	% difference	p-value[c]	ADO Z-score[d]
Tibial diaphysis					
Total vBMD (mg/cm3)	727 ± 70	1146 ± 120	+57.6%	<0.001	+6.0 (+5.0 to +7.0)
Cortical vBMD (mg/cm^3)	1147 ± 16	1209 ± 78	+5.4%	<0.001	+3.9 (+1.1 to +6.6)
Total BMC (mg/mm)	528 ± 64	687 ± 216	+30.1%	<0.01	+2.5 (+0.6 to +4.4)
Cortical BMC (mg/mm)	482 ± 62	666 ± 222	+38.0%	<0.001	+3.0 (+0.9 to +5.0)
Total area (cm^2)	7.31 ± 0.96	5.94 ± 1.51	−18.6%	<0.01	−1.4 (−2.3 to −0.5)
Cortical area (cm^2)	4.20 ± 0.52	5.46 ± 1.61	+29.9%	0.001	+2.4 (+0.6 to +4.2)
Medullary area (cm^2)	3.10 ± 0.76	0.49 ± 0.52	−84.3%	<0.001	−3.4 (−3.8 to −3.0)
Cortical area (% of total area)	57.9 ± 6.4	91.5 ± 9.4	+58.1%	<0.001	+5.3 (+4.4 to +6.1)
Cortical-to-medullary area ratio	1.4 ± 0.4	37.7 ± 42.6	+2539.9%	<0.001	+37.7 (+13.6 to +61.8)
Cortical thickness (mm)	5.35 ± 0.66	10.23 ± 2.59	+91.3%	<0.001	+7.4 (+5.2 to +9.6)
Distal tibia					
Total vBMD (mg/cm^3)	397 ± 45	762 ± 279	+91.8%	<0.001	+8.1 (+4.6 to +11.6)
Total BMC (mg/mm)	466 ± 59	770 ± 409	+65.3%	0.001	+5.2 (+1.2 to +9.1)
Total area (cm2)	11.81 ± 1.62	9.79 ± 2.27	−17.1%	<0.01	−1.2 (−2.0 to −0.5)

[a] Data are mean ± SD.

[b] Control data from male collegiate-level long jump and cross-country athletes (n=23) with a mean age=21.7±2.6 yrs, height=1.81±0.07 m, mass=73.3±9.0 kg [20].

[c] Determined using unpaired t-test

[d] Mean (95% confidence interval) z-score in ADO calculated against control

Table 3.

Bone turnover markers

Bone turnover markers	Min	Max	Mean	SD	Median
NTX/Creatinine ratio (nmol BCE/mmol Cr)	14	296	83	100	34
CTX (ng/mL)	0.15	1.57	0.50	0.40	0.40
P1NP (ng/mL)	25.6	1157.0	298.0	401.7	84.4
P1NP/CTX ratio	65.5	1446.3	481.7	381.5	358.4

Full biochemical profile of the cohort including distribution according to age groups is published separately in Imel, et al [18].